Geophys. J. Int. (2000) **143,** 700–708

Approximate retrieval of the point source in anisotropic media: numerical modelling by indirect parametrization of the source

Jan Šílený and Václav Vavryčuk

Geophysical Institute, Academy of Sciences of the Czech Republic, Boční II/1401, 141 31 *Praha* 4, *Czech Republic. E-mail: jsi@ig.cas.cz*

Accepted 2000 June 13. Received 2000 June 9; in original form 1999 May 26

SUMMARY

We propose an approximate approach to the waveform inversion of the mechanism and source time function of a point earthquake source buried in an anisotropic medium. We have modified the INPAR (INdirect PARametrization) inversion algorithm used for isotropic media by taking into account that the arrival times of waves propagating in an anisotropic medium differ from those propagating in an isotropic medium. All other effects caused by anisotropy are neglected. In the waveform inversion, we simply use the isotropic Green's function for constructing synthetic seismograms, and match them with anisotropic waveforms. To estimate the accuracy of this approach, we performed a series of numerical experiments covering various station configurations, ranging from very dense to sparse, and exploiting either only *P*, or both *P* and *S* waves. Treating anisotropy in this simplified way is mainly projected onto additional spurious moment tensor components, whilst the double-couple orientation and the source time function remain largely unaffected. It appears that even fairly high anisotropy (24 per cent in *P* waves and 11 per cent in *S* waves) can be treated by this approach without fatal loss of information about the source.

Key words: anisotropy, inversion, source parameters.

INTRODUCTION

Recent results of exploration and earthquake seismology have shown that the Earth's crust and upper mantle are often anisotropic (Leary *et al*. 1990; Babuška & Cara 1991; Hung & Forsyth 1999). Anisotropy of the crust is mostly caused by sediment layering, or by the alignment of fractures, cracks and microcracks associated with the stress history, deformation and faulting of the crust (Jones *et al*. 1999). Anisotropy of the mantle can be due to the preferred orientation of minerals such as olivine, or to melt-filled crack alignment. If the true structure is anisotropic, but we assume isotropic models, the waveform inversion for the source parameters may yield erroneous results. The errors may be large, particularly in local-scale studies, where waveforms are often significantly affected by anisotropy (Kaneshima *et al*. 1990; Holmes *et al*. 1993; Vavryčuk 1993; Coutant 1996; Tadakoro *et al*. 1999).

It is desirable, therefore, to use adequate anisotropic models for source parameter inversion; however, this task is complicated. First, forward modelling of waveforms in anisotropic media is more difficult than in isotropic media: *P*- and *S*-wave velocities are directionally dependent; *P*-wave polarization is not along a ray; and instead of one *S* wave, two *S* waves propagate under anisotropy (see Fig. 1), with different velocities and polarizations (see Fig. 2). Moreover, complications arise due to *S*-wave coupling (Chapman & Shearer 1989; Pšenčík 1998; Vavryčuk 1999) and due to the existence of *S*-wave singularities (Crampin 1991; Rümpker & Thomson 1994). Second, we need a large number of parameters to describe anisotropy properly; this is enormously demanding on the data used for determining the anisotropy. Therefore, the anisotropy of a medium is in most cases simplified: instead of a general anisotropy, we assume simple types of anisotropy such as transverse isotropy, and we

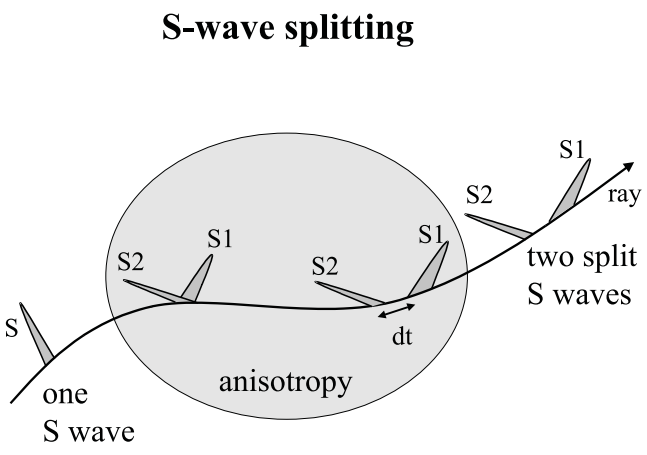

Figure 1. Schematic sketch of *S*-wave splitting in anisotropic media. Quantity *dt* denotes the delay time between the split *S* waves.

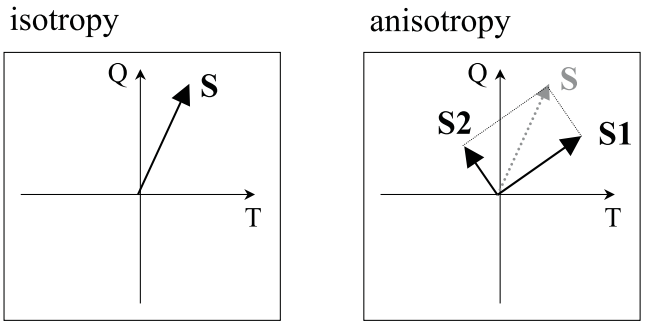

Figure 2. Polarization of split *S* waves in the plane perpendicular to the ray. S_1 and S_2 waves are approximately perpendicular.

often fix the orientation of the symmetry axis. Under these rather strong assumptions, we are able to recover some anisotropy parameters by *P*- and *S*-wave tomography (Chapman & Pratt 1992a,b; Jech & Pšenčík 1992), by analysis of *S*-wave splitting (Vavryčuk 1993), by analysis of *SKS* waves (Silver 1996; Kubo & Hiramatsu 1998), or by surface wave studies (Montagner 1994; Babuška *et al*. 1998).

Inversion of waveforms by using a simplified medium model was treated by Ramos-Martinez & McMehan (2000), who discussed the effects of inhomogeneity, anisotropy and viscoelasticity. However, they investigated a rather weak anisotropy which does not create an observable *S*-wave splitting in the configuration used. In this case, therefore, they reported only a minor influence of the anisotropy.

Taking into account that generating accurate Green's functions in anisotropic media is quite complicated, and that the anisotropy of real structures is unknown, or only roughly estimated, we propose an approximate approach to source parameter inversion in anisotropic media. We slightly modified the standard isotropic waveform inversion, considering anisotropy effects in a simple way, and use numerical experiments to test the accuracy of this approach.

METHOD

The INPAR inversion method (Šílený *et al*. 1992; Šílený 1997, 1998) is based on the INdirect PARametrization of the point source: moment tensor (MT) and source time function (STF) are determined using moment tensor rate functions (MTRFs). The method consists of two steps: (i) the inversion of waveforms for the independent MTRFs (Sipkin 1982); and (ii) the reduction of the MTRFs into MT and STF. The independent MTRFs represent, in general, a source whose mechanism varies with time. Reducing the MTRFs consists of selecting the correlated parts; the STF, in addition, is constrained to be non-negative. This procedure appears to provide a good estimate of the source, even if the medium inhomogeneity is modelled inexactly (Kravanja *et al*. 1999).

Synthetic seismograms calculated for an inexact model of the medium may mismatch the data as a result of differences in arrival times. Therefore, the synthetics need to be cross-correlated with the observed waveforms, and shifted to compensate for the arrival time differences. The search for an optimum shift for each station is carried out in most waveform inversion methods. However, inverting anisotropic waveforms using isotropic Green's functions requires independent time-shifts for each component of a three-component record. The modified INPAR method performs the cross-correlation automatically. Correlating each component independently is vital due to *S*-wave splitting: two *S* waves exist in an anisotropic waveform, whereas only a single *S* wave exists in an isotropic medium (Fig. 1). The key in our method is to match the dominant *S* wave in the anisotropic waveform with the single *S* wave of the isotropic synthetics. In Fig. 3, S_1 is the fast and S_2 is the slow *S* wave in an anisotropic medium. If the S_1 and S_2 waves have polarization directions coincident with the coordinate axes *x* and *y* (Fig. 3a), the S_1 and S_2 waves are projected into different components, and matching the single *S* wave of the isotropic synthetics is straightforward.

Similarly, no problems arise in the matching if the polarizations of the S_1 and S_2 waves are close to the coordinate axes (Fig. 3b), because one split *S* wave dominates in each component. However, if the S_1 and S_2 directions differ largely from the coordinate axes, the projected *S* waves have comparable amplitudes (Fig. 3c), and the matching is not unique. This is indeed the major source of error in inverting anisotropic waveforms using an isotropic model of the medium. The more frequent this pattern in the data set, the more biased the retrieved parameters of the source.

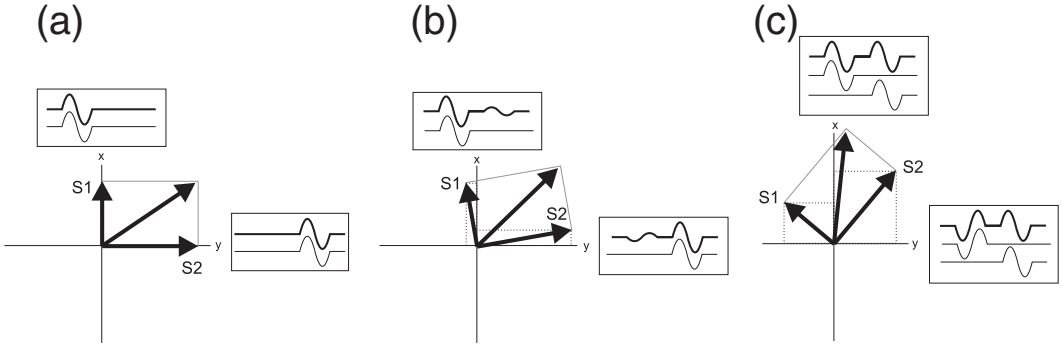

Figure 3. 2-D sketch of *S*-wave splitting in an anisotropic medium and schematic *S*-waveforms to be expected in the records (heavy lines) together with their hypothetical matching by isotropic synthetics (thin lines). The (*x*, *y*) plane represents the plane of *S*-wave polarization. (a) Waveforms in the direction of polarization of S_1 (fast) and S_2 (slow) wave. The matching by shifted isotropic synthetics is exact. (b) Waveforms along the coordinate axes (*x*, *y*) if they are close to the directions of polarization of the S_1 and S_2 waves. One of the split *S*-waves then dominates the record observed in the components *x* and *y*. The matching by isotropic synthetics is unique. (c) Waveforms along axes (*x*, *y*), which are far from the directions of polarization of the S_1 and S_2 waves. Both the split *S*-waves are then comparable in the *x* and *y* records. The matching by isotropic synthetics is not unique.

NUMERICAL EXPERIMENT—DATA

Anisotropic synthetic 'data' are calculated for a transversely isotropic medium with a vertical symmetry axis. Physically, the model corresponds to a system of dry parallel cracks (Hudson 1981). The *P*- and *S*-wave velocities and density of the host rock are $V_{P\text{-ROCK}} = 6.00$ km s^{-1}, $V_{S\text{-ROCK}} = 3.46$ km s^{-1} and $\rho = 3.30$ g cm^{-3}, and the crack density is $e = 0.1$. The corresponding density-normalized elastic parameters are $a_{11} = 34.36$, $a_{13} = 7.07$, $a_{33} = 21.20$, $a_{44} = 9.55$ and $a_{66} = 12.00$, using the 2-index matrix notation for the elasticity tensor (see Musgrave 1970, eq. 3.13.4). In the medium, *P*, *SV* and *SH* waves propagate with phase velocities dependent on the angle between the direction of propagation and the symmetry axis (see Fig. 4). The *SH* wave is faster than the *SV* wave for all directions except for the symmetry axis direction, where the velocities coincide. The angular variation in the phase velocity is almost 24 per cent for *P* waves, 1 per cent for *SV* waves and 11 per cent for *SH* waves, thus anisotropy is rather strong. The *P* and *SV* waves are polarized in the plane defined by the phase normal and the symmetry axis; however, they are not necessarily pure longitudinal and pure transverse waves, respectively. The polarization of the *SH* wave is perpendicular to the phase normal and to the symmetry axis.

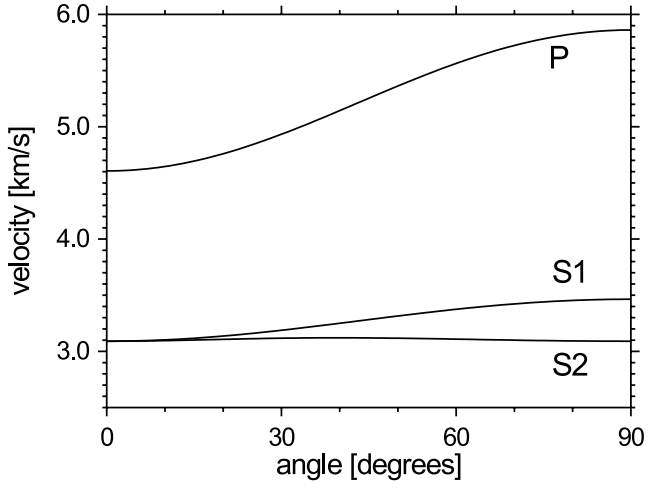

Figure 4. *P*-, S_1- and S_2-wave phase velocities as a function of the angle between the direction of propagation and the symmetry axis of the transversely isotropic medium.

The anisotropic wavefield generated by a point source in a homogeneous elastic medium is determined by calculating the integral solution numerically (see Burridge 1967, eq. 4.6; Wang & Achenbach 1994, eq. 13). The wavefield obtained is exact and complete, contains both far-field and near-field terms, and is valid for all distances and directions.

The station distribution simulates the network of seismo-acoustic sensors operating in the Underground Research Laboratory (URL) in Manitoba, Canada (Young & Collins 1993). 16 three-component accelerometers monitor the seismic activity induced by mining a tunnel in a nearly homogeneous granite rock. The aperture of the network is about 50 m and the source and station configuration corresponds to a hypocentre situated at the margin of the network (Fig. 5). The hypocentre distances range from 11 to 45 m and eight stations are below the hypocentre. The magnitudes of the events occurring in the URL range from −4 to −2 (Feignier & Young 1992), and the predominant frequency of the signals is about 1 kHz (Baker & Young 1997). The three-component sensors in the URL network are situated in boreholes drilled around the tunnel and their orientation is governed by the borehole direction. Before inverting real URL waveforms, they have to be rotated into the (N, E, Z) Cartesian system. However, for the purpose of this study, we generate synthetic 'data' immediately in the (N, E, Z) coordinates. Due to the general orientation of the stations with respect to the hypocentre investigated, all three components record both *P* and *S* waves (Fig. 6).

Station 1 is close to the hypocentre (12.4 m) and the split *S* waves are not separated yet. In the record of station 7 (27.5 m), the splitting can be observed well but the two *S* waves are not yet completely separated. Stations 12 and 16 are far enough away (40.7 and 45.4 m, respectively) for complete separation of the split *S* waves to occur.

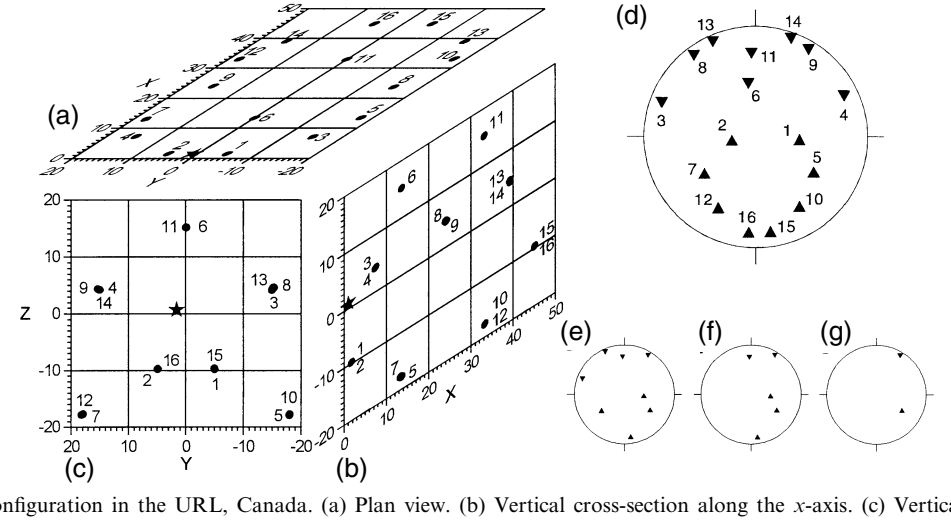

Figure 5. Station configuration in the URL, Canada. (a) Plan view. (b) Vertical cross-section along the *x*-axis. (c) Vertical cross-section along the *y*-axis, *, hypocentre; ●, stations, distances are in metres. (d) Equal area projection of lower focal hemisphere with all 16 stations of the network; ▲, stations below the hypocentre; ▼, stations above the hypocentre. (e–g) Reduced station configurations used in the synthetic tests, consisting of eight, five and two stations, respectively.

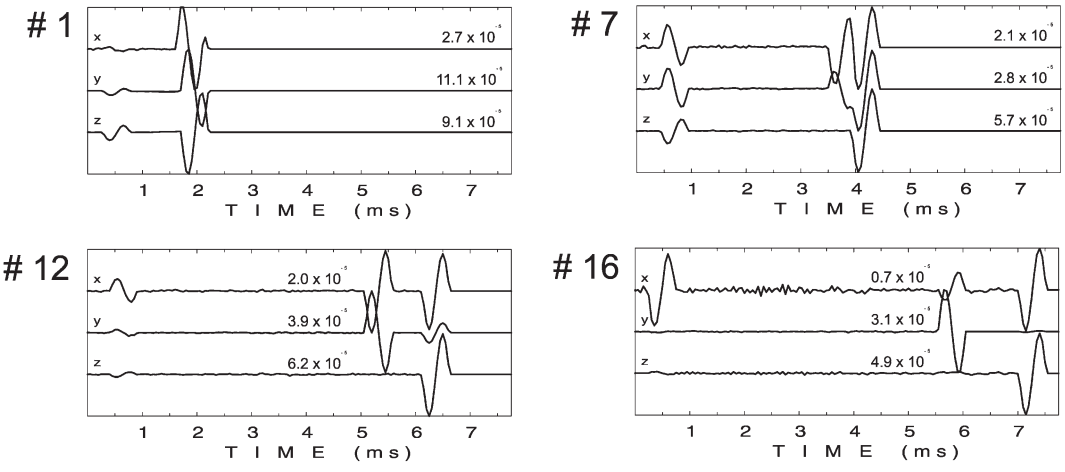

Figure 6. Three-component velocity seismograms at stations 1, 7, 12 and 16 at the distances 12.4, 27.5, 40.7 and 45.4 m, respectively.

To test the robustness of the modified INPAR algorithm, we consider station configurations ranging from a nearly perfect coverage of the focal sphere by all 16 stations to an extremely sparse coverage by two stations only (Figs 5d–g). Synthetic velocity records were generated for a pure shear-slip source (hereafter DC) consisting of equal amounts of dip-slip (thrust faulting) and strike-slip components described by the angles: dip $\delta=45^\circ$, strike $\phi=45^\circ$ and rake $\lambda=45^\circ$. The source time function is a sharp one-sided pulse (Fig. 7). In the synthetic experiments we invert the seismograms generated for an anisotropic model of the medium (Fig. 4) by assuming that the medium is isotropic, that is, we match anisotropic waveforms with synthetics constructed from isotropic Green's functions (Aki & Richards 1980, eq. 4.2.3).

NUMERICAL EXPERIMENT—RESULTS

Inversion of *P* waves

The anisotropic *P* wave is relatively simple: differences in arrival time relative to the isotropic case are compensated by cross-correlating synthetics and data; if the anisotropy is not extremely strong the polarization deviates little from the isotropic case. Numerical experiments inverting *P* waves generated by the DC source (Fig. 7) were performed with 16, eight and five stations (Figs 5d–f). In the last case a deviatoric constraint was applied because, with five independent data, we can search for five MT components only. The reconstruction of the STF is very good with all three configurations (Fig. 8): model inconsistencies are only reflected in a widening of the STF.

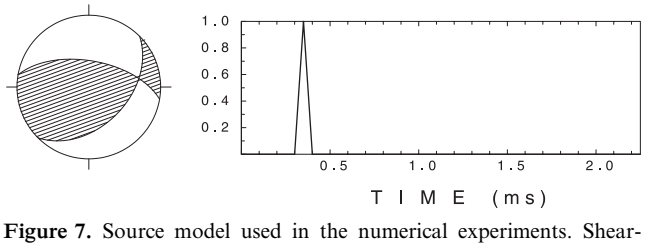

Figure 7. Source model used in the numerical experiments. Shear-slip source (hereinafter DC) containing equal amounts of strike-slip and dip-slip components: dip $\delta=45^\circ$, strike $\phi=45^\circ$ and rake $\lambda=45^\circ$. The source time function is a sharp one-sided pulse.

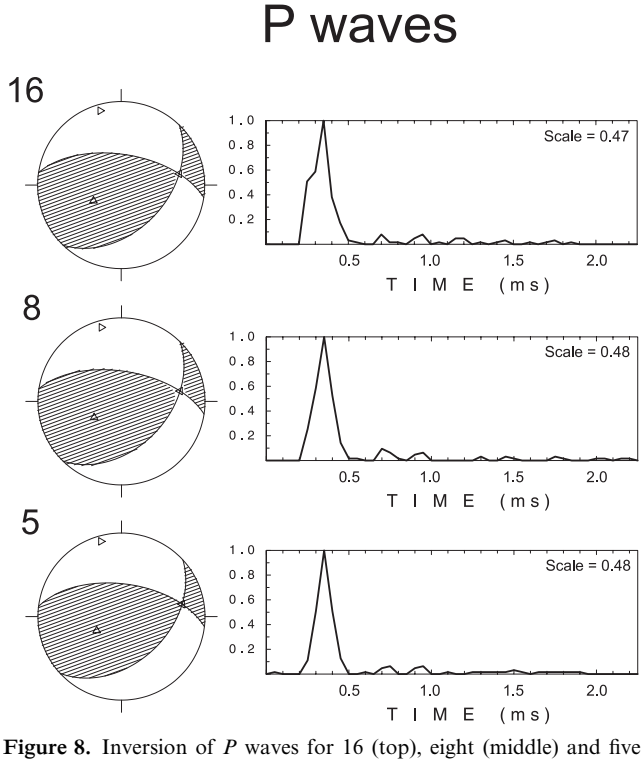

Figure 8. Inversion of *P* waves for 16 (top), eight (middle) and five stations (bottom; here the deviatoric constraint was applied). Left, retrieved mechanism; dashed area, compressions corresponding to the moment tensor; solid lines, nodal lines of the DC component; △, T-axis; ▷, P-axis; ◁, N-axis. Right, retrieved source time function.

However, this effect may only be significant for extremely short source time functions. If the STF extends over several sampling steps, it is of minor importance, because the widening represents only a small percentage of the STF duration (Fig. 9). The reconstructed STF is widened, but its amplitude is decreased in comparison with the input model (*cf.* Figs 7 and 8). Therefore, the scalar moment expressed as the integral of the STF over its total duration is not distorted too much with respect to the input value (Table 1). The orientation of the mechanism is determined very well in all three configurations tested. However, a small spurious source component, which is mostly a compensated linear vector dipole (CLVD), appears in all the cases.

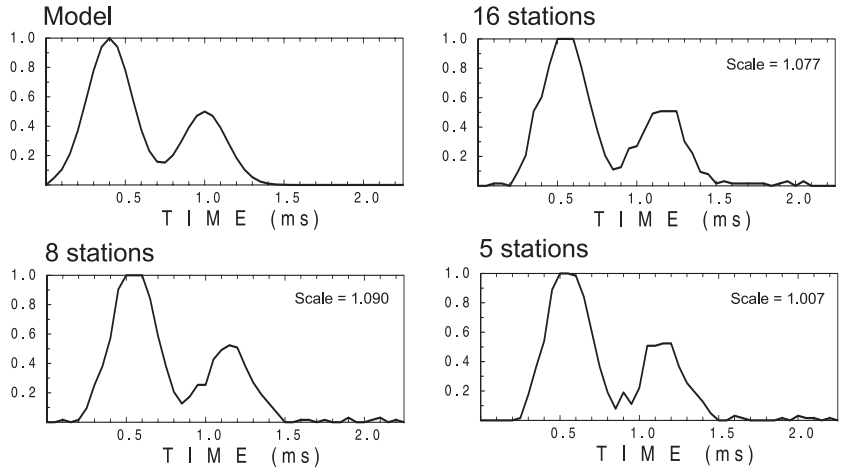

Figure 9. Source time function retrieved from anisotropic *P* wave inversion using 16, eight and five stations, compared with the input model simulating a smooth double pulse.

Table 1. Scalar moment (normalized to the value of M_0 of the input model) determined from *P* waves only (upper row), and from both *P* and *S* waves.

Number of stations	16	8	5	2
P	1.50	1.44	1.33	
P+*S*	1.32	1.41	1.34	1.15

Inversion of *P* and *S* waves

Using three-component sensors, each station provides *P*, *SV* and *SH* waves. Thus, contrary to exploiting only *P* waves, where six stations are necessary to retrieve six MT components, we can now retrieve the complete moment tensor from two stations only. This is the principal benefit of adding *S* waves to the data set. However, adding *S* waves introduces a problem not encountered with *P* waves, namely *S*-wave splitting. Due to splitting, polarization of each split *S* wave is determined by the medium properties and not by the source. To use the *S* waves for source determination, we have to combine the split *S* waves to reconstruct the original isotropic wave. This can be done prior to inversion, if the delay between the split *S* waves is known and corrected for (Karnassopoulou *et al.* 1996). The modified INPAR algorithm effectively corrects for the split *S* waves by determining the time-shift between synthetic and observed records and by applying the time-shift to achieve the best alignment. Shifting is performed for each component independently.

Fig. 10 demonstrates the matching *S*-wave isotropic synthetics to the anisotropic data for stations 1, 7, 12 and 16 for the 16-station experiment (Fig. 5d). Fig. 6 shows the complete anisotropic waveforms—including *P* and *S* waves—for these stations. Since station 1 is close to the hypocentre, the split *S* waves are not separated in time yet, and effectively behave as an isotropic *S*-wave. Therefore, the match with isotropic synthetics is very good. The remaining stations 7, 12 and 16 clearly exhibit *S*-wave splitting. The pattern discussed in Fig. 3(b) is demonstrated in station 16, where the matching with isotropic

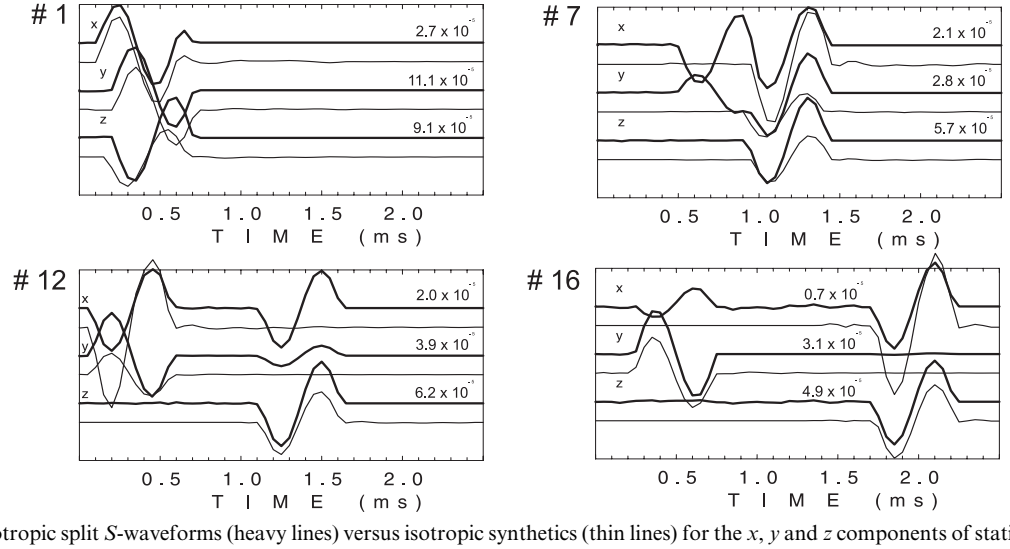

Figure 10. Anisotropic split *S*-waveforms (heavy lines) versus isotropic synthetics (thin lines) for the *x*, *y* and *z* components of stations 1, 7, 12 and 16 in the experiment inverting *P* and *S* waves from 16 stations of the URL network. The number attached to each component specifies the maximum amplitude of the channel.

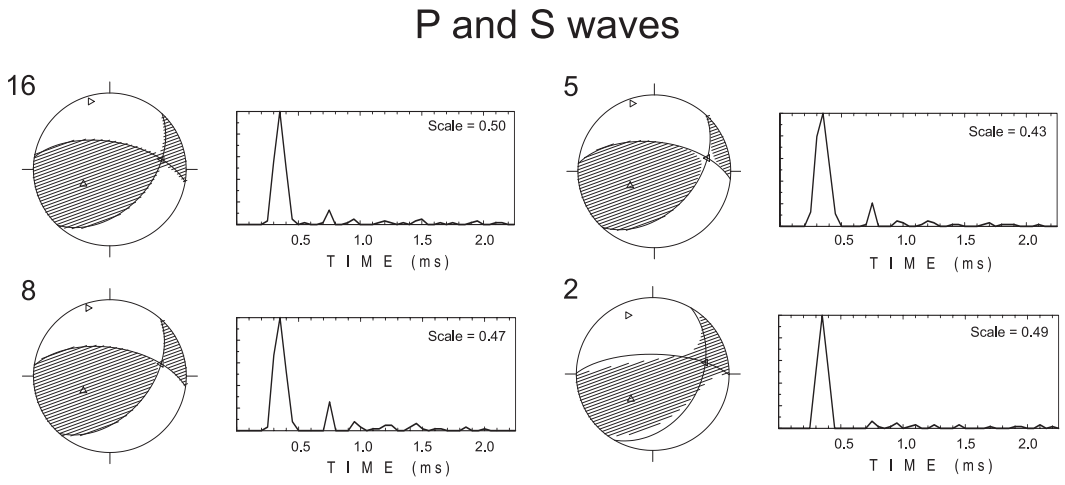

Figure 11. Results of inversion of both *P* and *S* waves for the 16-, eight-, five- and 2-station configurations. For details, see the caption of Figure 7.

synthetics is straightforward; similarly for the *z*-component of stations 7 and 12, and partly for the *y*-component of station 12. The pattern discussed in Fig. 3(c) is demonstrated by the *x*-component of stations 7 and 12, and by the *y*-component of station 7. In these cases the matching with isotropic synthetics containing the single *S* wave cannot be satisfactory: one of the two *S* waves is matched, the other is ignored. Thus, the earlier *S* wave is ignored in the *x*- and *y*-components of station 7, whilst the later one is matched, and *vice versa* in the *x*-component of station 12.

Inverting both *P* and *S* waves together, we investigated all station configurations, (d)–(g) in Fig. 5. In all cases, the reconstructed STF is only affected a little. Source mechanism retrieval is very good for all configurations. Similarly to the *P*-wave inversion, inconsistencies are reflected in the appearance of a spurious CLVD and volumetric source component (V) (Fig. 11). The reconstructed STF is slightly widened by neglecting anisotropy, and its amplitude is reduced with respect to the input model. The retrieved scalar moment, however, does not differ much from the input model (Table 1).

Obviously, the success of the method depends on the source mechanism, as it rules the amplitudes of the phases at individual stations. Thus, the number of poorly matched *S* patterns (presence of both split waves in a single component) depends on the mechanism in a fixed station configuration. We have performed a large set of numerical experiments (about 1500) with randomly generated shear mechanisms to estimate the resolving capabilities of the method. Fig. 12 shows the average deviation of the principal axes of the retrieved mechanism relative to the input DC model, the percentage of spurious V and CLVD components, and the normalized correlation coefficient of the input STF (Fig. 7) and the resolved STF. The statistics are constructed for the 16-station and two-station configurations. The deviation of the principal axes is small and narrowly centred for 16 stations (around 4°); for the two-station inversion the deviation is large (peak $>10°$) and has a long tail. A similar conclusion applies to the spurious V and CLVD source components. The histograms of the correlation coefficient of the input STF and the reconstructed STF are close for both the station configurations investigated. The rather small value, around 0.4, reflects the widening of the reconstructed STF. The large drop in the correlation coefficient is caused by the difference in shape of the sharp peaked input STF and the widened reconstructed STF. The drop in the correlation function would be smaller for a longer STF (see Fig. 9).

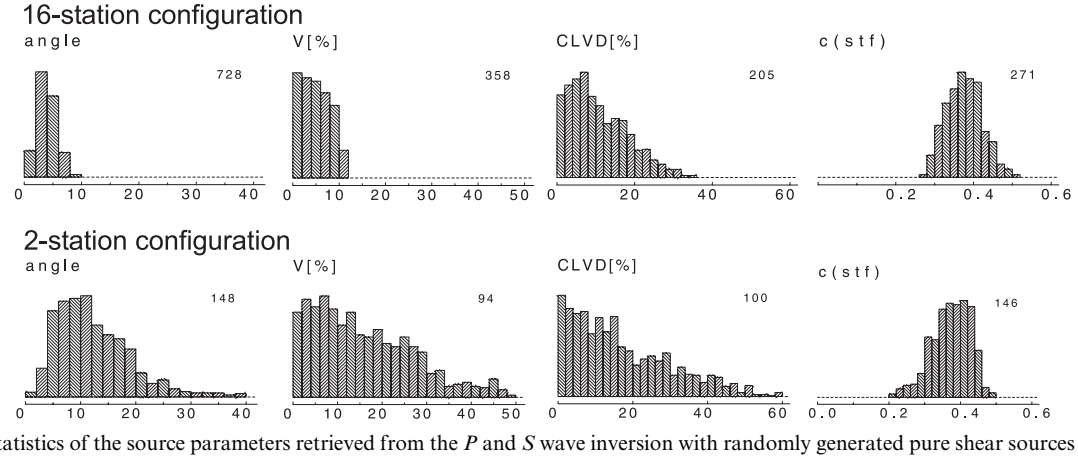

Figure 12. Statistics of the source parameters retrieved from the *P* and *S* wave inversion with randomly generated pure shear sources for the 16- and two-station configurations. From left to right: histogram of the average deviation in degrees of the DC orientation (arithmetic mean of the three inclination angle differences between input and retrieved principal axes); spurious V component (in percentage); spurious CLVD component (in percentage), correlation coefficient of the reconstructed STF and the input model. Number next to each histogram—number of experiments yielding the most frequent solution (maximum bar height), a total of about 1500 tests were performed.

To summarize, given a sufficient number of stations, the deviation of the source orientation is negligible; the distortion of the mechanism is projected into the V and CLVD components; and the retrieved STF is widened, but the scalar moment is estimated fairly well.

INVERSION OF THE URL EVENT OF 1992 FEBRUARY 25, AT 20:58:00

Seismic observations indicate that the rock massif in the URL is anisotropic: measurement of the *P*-wave velocity indicates its directional dependence, and the *S*-wave pattern indicates anisotropic splitting (Holmes *et al.* 1993). However, the measurements are not detailed enough to allow the characteristics of the anisotropy—its symmetry, orientation and strength—to be determined. Thus, the application of the INPAR method may be advantageous here.

As an example, we have processed the event of 1992 February 25 at 20:58:00. The event of moment magnitude -3.6 was located at the hypocentre of the event investigated in the synthetic tests (Fig. 5). We calculated isotropic Green's functions for a homogeneous medium ($V_P = 6$ km s^{-1}, $V_S = 3.464$ km s^{-1}, $\rho = 2.9$ g cm^{-3}) and low-pass filtered them (cut-off frequency at 10 kHz) to model the frequency content of the waveforms properly. We performed four inversions with different data sets ranging from the complete data set available (*P* and *S* at seven stations) to a reduced data set consisting of *P* and *S* at two stations only; see Figs 13(a)–(d), left column.

The source retrieval confirms the conclusion drawn from the synthetic tests. The inversions with *P* and *S* waves from seven and three stations yield a fairly stable orientation of the mechanism's DC part, whilst the amount of additional source components V and CLVD, expressed in the size of the zones of compression and dilatation, varies largely (Fig. 13, middle). Data from two stations are insufficient to determine the orientation of the DC part of the mechanism reliably. The retrieved STF is remarkably stable for all configurations treated (Fig. 13, right-hand column).

Fig. 14 shows an example of the match between isotropic synthetics and observed records in the window containing the split *S* waves. For station 13 (Fig. 5), the fast *S* wave (S_1) prevails in the *z*-component, whilst the slow *S* wave (S_2) dominates in the *x*-component. The complex anisotropic waveforms are matched with isotropic synthetics, allowing the balancing of the arrival time differences between the S_1 and S_2 phases. The isotropic synthetics model the dominant parts of the waveforms in the *x*- and *z*-components well.

DISCUSSION

The synthetic tests demonstrated that the INPAR algorithm, modified to allow the time-shifts for each component individually, provides robust results even in the presence of anisotropy. As expected, inversion of *P* waves yields a good reconstruction of the source, because isotropic and anisotropic *P*-waveforms are similar. It is sufficient to compensate for the differences

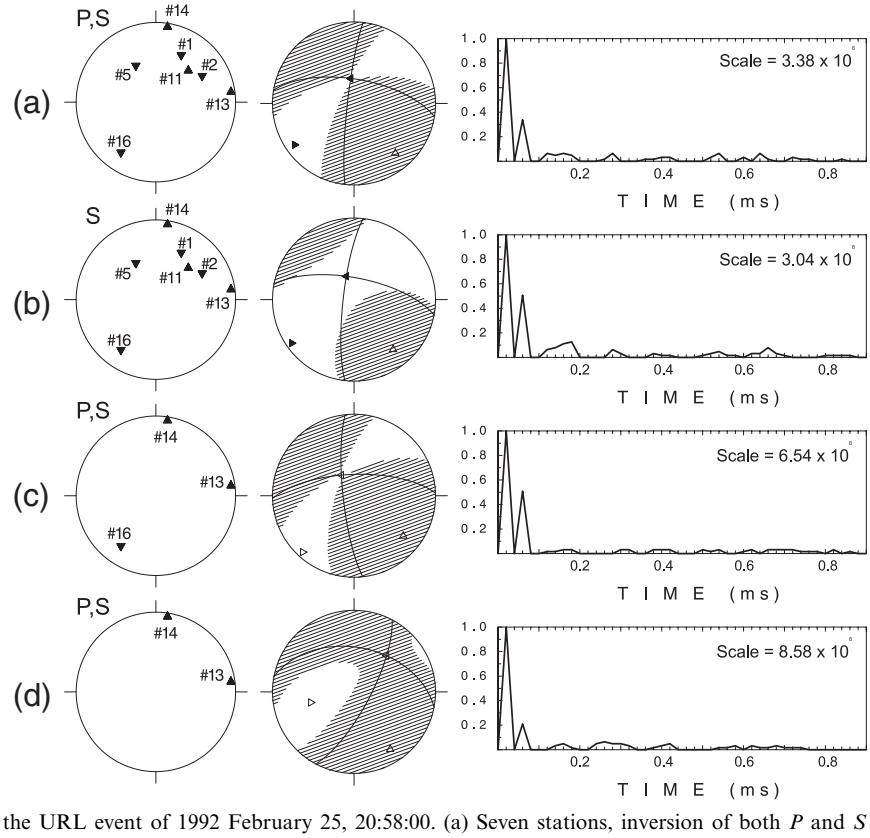

Figure 13. Inversion of the URL event of 1992 February 25, 20:58:00. (a) Seven stations, inversion of both *P* and *S* waves. (b) Seven stations, inversion of *S* waves only. (c) Three stations, *P* and *S* waves. (d) Two stations, *P* and *S* waves. Left column, station distribution on the focal sphere; middle column, *P*-radiation pattern of the retrieved mechanism (convention as in Fig. 8); right-hand column, source time function.

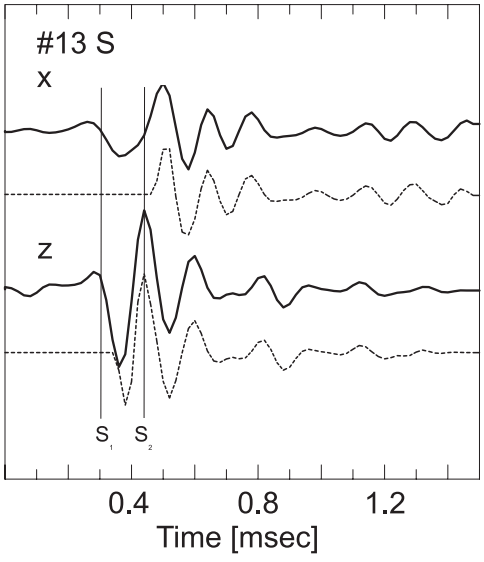

Figure 14. Match of the synthetics to the data (URL event, 1992 February 25, 20:58:00) for the *x*- and *z*-components at station 13 (Fig. 5). Heavy solid line, observed velocity records; thin dashed line, synthetics; vertical lines mark the S_1 and S_2 wave arrivals picked in the records.

in arrival times due to the directional dependence of the propagation velocity. Exploiting *S* waves is more complicated because of *S*-wave splitting in an anisotropic medium. This effect can be partly compensated for by allowing independent time-shifts for each component. In this case, the algorithm matches the isotropic *S* wave to that part of the split *S* wave which is dominant. This simplification cannot eliminate the effects of *S*-wave splitting completely and leads to distortion of the STF. This distortion, however, is not essential, being manifested by a small widening of the true source signal. The benefit of adding *S* waves is a substantial reduction in the number of stations required. Whilst six stations are necessary to retrieve the complete moment tensor from *P* waves, two three-component stations are sufficient if both *P* and *S* waves are available. Therefore, we suggest the following strategy when using our inversion method for data which show strong anisotropy. If the number of stations is large, it is better to avoid exploiting *S* waves and invert only *P* waves because their anisotropic delays are compensated for, and their shape does not differ much from isotropic *P* waves. In the case where only a few stations are available, *S* waves can also be included. We should, however, be careful to eliminate the records where both split *S* waves are present with comparable amplitudes.

The double-couple part of the mechanism and the STF are well retrieved even when the waveforms display clear *S*-wave splitting and stations cover the focal sphere only sparsely. The simplified treatment under anisotropy mainly results in contaminating the source by spurious components: for a DC mechanism, spurious V and CLVD components appear. The size of the spurious components decreases with an increasing number of stations, but remains considerable even for a very dense network (16 stations). The DC orientation, however, is not biased much, provided that a reasonable network configuration is available. This encouraging result is true even for fairly high degrees of anisotropy. The tests investigated one particular type of anisotropy—a transversely isotropic medium with a vertical axis of symmetry. Since all major complexities of seismic wave propagation caused by anisotropy were present (dependence of the propagation velocity on direction, *P* and *S* waves not being purely longitudinal and transverse, respectively, *S*-wave splitting), we expect the INPAR algorithm to perform well for other types of anisotropy as well.

It is known that the V and CLVD components of the source retrieved by inverting seismic records may often be spurious phenomena originated by mis-modelling an inhomogeneous medium (Kravanja *et al*. 1999) or by over-simplifying the seismic source (Frohlich 1994). We have shown that neglecting anisotropy may be an additional reason for the appearance of spurious non-DC components of the source in waveform inversion.

All numerical experiments were performed for homogeneous media, since we focused on problems of anisotropy versus isotropy and tried to avoid complications due to the inhomogeneity of the medium. Thus, the conclusions are valid for set-ups where the inhomogeneity of the medium between the focus and the stations is low, that is, for local studies in simple geological environments such as the Underground Research Laboratory. Extension to seismological scale requires verification by further synthetic experiments including the inhomogeneity of the medium.

ACKNOWLEDGMENTS

The study was partly supported by the EC-INCO-Copernicus Grant #IC 15 CT96 200, the Acad. Sci. Czech Rep. Grant Agency Grant #A3012904, and by the Czech Rep. Grant Agency Grant #205/00/1350. The authors wish to thank Prof. R. P. Young, University of Liverpool, UK, for providing them with the records of the URL event, and an anonymous reviewer for numerous helpful comments. Part of the study was carried out when JS was at the Abdus Salam ICTP at Trieste, Italy, within the scope of the Associated Membership Scheme.

REFERENCES

Aki, K. & Richards, P.G., 1980. *Quantitative Seismology,* Freeman, San Francisco.

Babuška, V. & Cara, M., 1991. *Seismic Anisotropy in the Earth,* Kluwer Academic Publishers, London.

Babuška, V., Montagner, J.P., Plomerová, J. & Girardin, N., 1998. Age-dependent large-scale fabric of the mantle lithosphere as derived from surface-wave velocity anisotropy, *Pure appl. Geophys.,* **151,** 257–280.

Baker, C. & Young, R.P., 1997. Evidence for extensile crack initiation in point source time-dependent moment tensor solutions, *Bull. seism. Soc. Am.,* **87,** 1442–1453.

Burridge, R., 1967. The singularity on the plane lids of the wave surface of elastic media with cubic symmetry, *Q. J. Mech. appl. Math.,* **20,** 41–56.

Chapman, C.H. & Pratt, R.G., 1992a. Traveltime tomography in anisotropic media I: Theory, *Geophys. J. Int.,* **109,** 1–19.

Chapman, C.H. & Pratt, R.G., 1992b. Traveltime tomography in anisotropic media II: application, *Geophys J Int.,* **109,** 20–37.

Chapman, C.H. & Shearer, P.M., 1989. Ray tracing in azimuthally anisotropic media—II, Quasi-shear wave coupling, *Geophys J.,* **96,** 65–83.

Coutant, O., 1996. Observation of shallow anisotropy on local earthquake records at the Garner Valley, Southern California, downhole array, *Bull. seism. Soc. Am.,* **86,** 477–488.

Crampin, S., 1991. Effects of point singularities on shear-wave propagation in sedimentary basins, *Geophys. J. Int.,* **107,** 531–543.

Feignier, B. & Young, R.P., 1992. Moment tensor inversion of induced microseismic events: evidence of non-shear failures in the $-4 < M < -2$ moment magnitude range, *Geophys. Res. Lett.,* **19,** 1503–1506.

Frohlich, C., 1994. Earthquakes with non-double-couple mechanisms, *Science,* **264,** 804–809.

Holmes, G.M., Crampin, S. & Young, R.P., 1993. Preliminary analysis of shear-wave splitting in granite at the Underground Research Laboratory, Manitoba, *Canad. J. Explor. Geophys.,* **29,** 140–152.

Hudson, J.A., 1981. Wave speeds and attenuation of elastic waves in material containing cracks, *Geophys. J. R. astr. Soc.,* **64,** 133–150.

Hung, S.-H. & Forsyth, D.W., 1999. Anisotropy in the oceanic lithosphere from study of local intraplate earthquakes on the west flank of the southern East Pacific Rise: Shear wave splitting and waveform modeling, *J. Geophys. Res.,* **104,** 10.695–10.717.

Jech, J. & Pšenčík, I., 1992. Kinematic inversion for qP and qS waves in inhomogeneous anisotropic structures, *Geophys. J. Int.,* **108,** 604–612; Erratum, 1992, *Geophys. J. Int.,* **110,** 397.

Jones, K., Warner, M. & Brittan, J., 1999. Anisotropy in multi-offset deep-crustal seismic experiments, *Geophys. J. Int.,* **138,** 300–318.

Kaneshima, S., Maeda, N. & Ando, M., 1990. Evidence for the splitting of shear waves from waveforms and focal mechanism analyses, *Phys. Earth planet. Inter.,* **61,** 238–252.

Karnassopoulou, A., Pierce, R.G. & Booth, D.C., 1996. A method to determine microearthquake focal mechanism in the presence of seismic anisotropy, *Tectonophysics,* **261,** 115–126.

Kravanja, S., Panza, G.F. & Šílený, J., 1999. Robust retrieval of a seismic point-source time function, *Geophys. J. Int.,* **136,** 385–394.

Kubo, A. & Hiramatsu, Y., 1998. On presence of seismic anisotropy in the Asthenosphere beneath continents and its dependence on plate velocity: Significance of reference frame selection, *Pure appl. Geophys.,* **151,** 281–303.

Leary, P.C., Crampin, S. & McEvilly, T.V., 1990. Seismic fracture anisotropy in the Earth's crust: an overview, *J. geophys. Res.,* **95,** 11.105–11.114.

Montagner, J.P., 1994. What can seismology tell us about mantle convection? *Rev. Geophys.,* **32,** 115–137.

Musgrave, M.J.P., 1970. *Crystal Acoustics,* Holden-Day, San Francisco.

Pšenčík, I., 1998. Green's functions for inhomogeneous weakly anisotropic media, *Geophys. J. Int.,* **135,** 279–288.

Ramos-Martinez, J. & McMehan, G.A., 2000. Source parameter estimation by full waveform inversion in 3D heterogeneous visco-elastic anisotropic media, *Bull. seism. Soc. Am.*, in press.

Rümpker, G. & Thomson, C.J., 1994. Seismic-waveforms effects of conical points in gradually varying anisotropic media, *Geophys. J. Int.,* **118,** 759–780.

Šílený, J., 1997. Moment tensor rate functions from waveforms with non-homogeneous variance, *Geophys. J. Int.,* **131,** 767–769.

Šílený, J., 1998. Earthquake source parameters and their confidence regions by a genetic algorithm with a 'memory', *Geophys. J. Int.,* **134,** 228–242.

Šílený, J., Panza, G.F. & Campus, P., 1992. Waveform inversion for point source moment tensor retrieval with variable hypocentral depth and structural model, *Geophys. J. Int.,* **109,** 259–274.

Silver, P.G., 1996. Seismic anisotropy beneath the continents: Probing the depths of geology, *Ann. Rev. Earth planet. Sci.,* **24,** 385–432.

Sipkin, S.A., 1982. Estimation of earthquake source parameters by the inversion of waveform data: synthetic waveforms, *Phys. Earth planet. Inter.,* **30,** 242–259.

Tadakoro, K., Ando, M. & Umeda, Y., 1999. S wave splitting in the aftershock region of the 1995 Hyogo-ken Nanbu earthquake, *J. geophys. Res.,* **104,** 981–991.

Vavryčuk, V., 1993. Crustal anisotropy from local observations of shear-wave splitting in West Bohemia, Czech Republic, *Bull. seism. Soc. Am.,* **83,** 1420–1441.

Vavryčuk, V., 1999. Applicability of higher-order ray theory for S-wave propagation in elastic weakly anisotropic inhomogeneous media, *J. geophys. Res.,* **104,** 28.829–28.840.

Wang, C.-Y. & Achenbach, J.D., 1994. Elastodynamic fundamental solutions for anisotropic solids, *Geophys. J. Int.,* **118,** 384–392.

Young, R.P. & Collins, D.S., 1993. The spatial and temporal distribution of AE/MS source locations following the mine-by tunnel excavation of round 17, Rept #RP017AECL, Atomic Energy Canada Ltd, Kingston.